Caspian Journal of Environmental Sciences
Online ISSN: 1735-3866
Print ISSN: 1735-3033

Spatiotemporal Analysis of Land Surface Temperature (LST) and Normalized Difference Vegetation Index (NDVI) Dynamics in Central Guilan, Iran (1989–2023)

Seyyed Mahmood Hashemi*, Seyyedeh Masoumeh Taherzadeh Kouzani

Department of Environment, Faculty of Natural Resources, University of Guilan, Sowme-Sara, Guilan, Iran

* *Corresponding Author's Email: hashemism@guilan.ac.ir, hashemeesm@gmail.com*

ABSTRACT

This study investigates the spatiotemporal dynamics of land surface temperature (LST) and vegetation cover, represented by the Normalized Difference Vegetation Index (NDVI), in Central Guilan Province, Northern Iran, a core part of the relic Hyrcanian biome, from 1989 to 2023. LST was retrieved from Landsat 5 TM and Landsat 8 OLI/TIRS, while NDVI was derived from red and near-infrared bands. Spatial autocorrelation of LST was assessed with Global Moran's I, and Pearson correlation was applied to quantify LST–NDVI relationships. Results show a marked rise in mean LST from 18.48 °C in 1989 to 23.13 °C in 2023. Strong negative correlations between LST and NDVI were identified (r = –0.718 in 1989; r = –0.743 in 2023), confirming vegetation's key role in regulating surface temperatures. Spatial clustering of thermal anomalies was intensified during the study period, with Moran's I increasing from 0.39 to 0.68, indicating urban heat island (UHI) expansion. These findings demonstrate that how land transformation has altered regional microclimates and highlight the urgent need for sustainable planning to enhance climate resilience. Given Central Guilan's location within the globally valuable Hyrcanian biome, effective conservation and adaptive land management are essential to protect its ecological integrity under ongoing climate and land-use pressures.

Keywords: Land surface temperature (LST), NDVI, Moran's I, Urban heat islands, Guilan Province.
Article type: Research Article.

INTRODUCTION

The interaction between land surface temperature (LST) and vegetation cover plays a pivotal role in regulating terrestrial ecosystem processes, particularly in areas undergoing rapid environmental transformation (Cracknell 2007). Vegetation affects LST through biophysical mechanisms such as evapotranspiration and canopy shading, whereas LST serves as a key indicator of surface energy fluxes influenced by both natural and anthropogenic drivers (Elachi & Van Zyl 2021). The Normalized Difference Vegetation Index (NDVI), derived from satellite remote sensing, remains a widely utilized proxy for assessing vegetation health and density, enabling the temporal analysis of vegetation–climate dynamics (Eastman 2009). Rapid urbanization has intensified urban heat islands (UHIs), where cities are significantly warmer than nearby rural areas (Rizwan & Dennis 2008). Current projections suggest that by 2050, approximately 68% of the global population will reside in urban environments (UN 2018), exacerbating energy demand and public health vulnerabilities (Santamouris 2020). Addressing these challenges aligns with the Sustainable Development Goals (SDGs), particularly SDG 11 (Sustainable Cities) and SDG 13 (Climate Action), which advocate for integrated urban planning and the expansion of green infrastructure to mitigate UHI effects (UN 2015). In Iran, the urban population has grown at an average annual rate of 4.2% since 2000. Guilan Province, located along the Southwest Caspian Sea coast, has witnessed a 25% population increase since 1990 (Statistical Center of Iran 2016). This demographic growth has triggered substantial land use changes, including the conversion of forests and wetlands into impervious surfaces, thereby disrupting local

hydrological cycles and elevating LST (Aghsaei *et al.* 2020). These transformations pose serious threats to food security (SDG 2) and aquatic ecosystems (SDG 14; FAO 2021). Recent spatial analyses in the region have documented these trends, revealing significant LST increases concurrent with land degradation (Fallah Ghalhari & Dadashi Roudbari 2018). Central Guilan, characterized by Hyrcanian forests, wetlands, and agricultural plains, has experienced extensive land cover modifications over the past three decades (Shooshtari & Gholamalifard 2015). These alterations have reshaped local energy balances and ecological processes (Ellis 2015). The magnitude of these transformations is particularly pronounced in the ecologically sensitive Hyrcanian lowlands (Shakiba *et al.* 2024). Landscape ecology frameworks provide valuable insights into these dynamics, emphasizing the role of spatial configurations of natural and anthropogenic elements in mediating ecosystem functioning and energy transfer (Forman & Godron 1986; Naveh & Lieberman 1994). Remote sensing (RS) and geographic information systems (GIS) have become indispensable tools for monitoring and analyzing spatiotemporal patterns in land surface conditions (Lillesand *et al.* 2015). Landsat satellite data, which have consistently provided NDVI and thermal information since the 1980s, are especially valuable for long-term environmental assessments (Roy *et al.* 2014). Furthermore, spatial statistical techniques such as Moran's I enhance analytical precision by quantifying spatial autocorrelation and detecting clusters of elevated LST associated with landscape transitions (Weng 2009). The NDVI–LST relationship serves as a critical metric for understanding vegetation–climate interactions. For instance, Guha *et al.* (2018) reported that NDVI explained a substantial portion of LST variability across vegetation types, while Zhu *et al.* (2022) demonstrated the efficacy of urban greening in reducing LST across Chinese cities. In Northern Iran, the expansion of impervious surfaces has been linked to increased LST and a concurrent decline in NDVI, with the Caspian lowlands exemplifying this trend (Azadeh & Etemadi Kia 2024). A similar pattern has been observed in Tehran, where vegetation loss has weakened the NDVI–LST coupling, intensifying urban thermal anomalies (Karimi Firozjaei *et al.* 2025). On a broader geographic scale, afforestation initiatives have effectively reduced surface temperatures in Mediterranean regions (Delgado-Capel *et al.* 2024), while NDVI–LST linkages have proven useful for assessing drought impacts in arid environments (Rahimi *et al.* 2025). Recent studies employing advanced spatial analysis methods, including Moran's I, have successfully captured the spatial heterogeneity of NDVI–LST interactions in complex landscapes (Alademomi *et al.* 2022). In this context, the spatial variability of landscape patterns in Guilan's physiotopes and ecotopes necessitates refined analytical approaches to better understanding vegetation–thermal dynamics. Accordingly, this study investigates the spatiotemporal NDVI–LST relationship in Central Guilan Province from 1989 to 2023 using Landsat imagery and spatial statistical methods. The findings aim to inform climate-resilient land-use planning and foster sustainable landscape management in this ecologically critical region.

MATERIALS AND METHODS

LST was estimated from Landsat 5 Thematic Mapper (TM) and Landsat 8 Operational Land Imager/Thermal Infrared Sensor (OLI/TIRS) data following a multi-step process involving radiometric calibration, atmospheric correction, and land surface emissivity (LSE) estimation. The processing was conducted using RS and GIS software tools such as ENVI, ArcGIS Pro, and open-source Python scripts.

Study area

The study focuses on the central region of Guilan Province, located in Northern Iran along the southern coast of the Caspian Sea. This region is characterized by a temperate and humid climate that supports dense vegetation, including remnants of the ancient Hyrcanian mixed forests (Yavari *et al.* 2012). Over recent decades, the area has experienced rapid population growth, urban expansion, and land use changes, making it a suitable case for examining vegetation–climate interactions. The region includes diverse landscapes such as Hyrcanian forests, wetlands, and agricultural plains. Over the past three decades, deforestation and urbanization have significantly altered the region's hydrology and microclimates (Abdollahi 2019; Haghighi Khomami *et al.* 2023).

Preprocessing and data acquisition

In this study, satellite imageries from Landsat 5 (1989) and Landsat 8 (2023) obtained from the United States Geological Survey (USGS) EarthExplorer platform were utilized. Level-1 terrain-corrected (L1T) imagery was used to ensure geometric accuracy and radiometric consistency (USGS 2021). The images were selected in a manner that allows clear identification and comparison of vegetation cover and other surface features across the two time points. To ensure temporal consistency, cloud-free images (with less than 10% cloud cover)

corresponding to the same season were selected for both sensors, specifically within a one-month time window in May of each year. This selection minimizes atmospheric and seasonal variation, thereby improving the accuracy of LST and NDVI calculations. For LST analysis, the thermal bands of Landsat 5 TM (Band 6), with a native spatial resolution of 120 meters, and Landsat 8 TIRS (Bands 10 and 11), with a native resolution of 100 meters, were used. Detailed specifications of the satellite imagery used are presented in Table 1. Atmospheric correction and image preprocessing were performed using standard protocols in Google Earth Engine. NDVI was computed from the red and near-infrared bands, while LST was retrieved using the thermal infrared bands with radiometric calibration and emissivity correction procedures. Spatial autocorrelation of LST values was assessed using Moran's I index to detect clustering patterns indicative of UHIs. Pearson correlation analysis was applied to evaluate the relationship between NDVI and LST for both years. All geospatial analyses were conducted using ArcGIS and QGIS platforms.

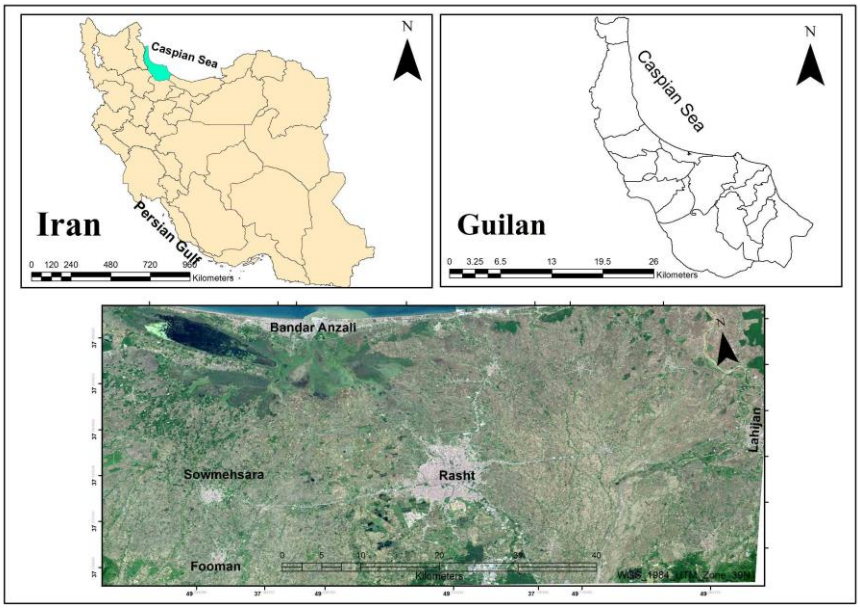

Fig. 1. Study area in Central Guilan Province, Iran, defined by the coordinates (1) 37.01°N, 49.92°E; (2) 37.42°N, 50.01°E; (3) 37.54°N, 49.23°E; and (4) 37.22°N, 49.14°E.

Table 1. Specifications of the satellite imagery and sensors used in this study.

Satellite	Resolution	Sensor	Path/Row	Acquisition Date	Coordinate System
Landsat 5	Resampled to 30 m	TM	166/34	1989-05-04	WGS 1984/UTM Zone 39N
Landsat 8	Resampled to 30 m	OLI/TIRS	166/34	2023-05-05	WGS 1984 / UTM Zone 39N

Source: United States Geological Survey (USGS Landsat data archive: https://landsat.usgs.gov).

LST derivation

LST was derived for the years 1989 and 2023 using satellite imagery from the Landsat 5 Thematic Mapper (TM) and Landsat 8 Operational Land Imager/Thermal Infrared Sensor (OLI/TIRS), respectively. For the 1989 dataset, LST was calculated using the well-established single-channel algorithm, which is commonly employed for analyzing thermal infrared data in long-term surface temperature studies (Avdan & Jovanovska 2016). In contrast, the 2023 Landsat 8 data utilized the split-window algorithm, which incorporates both thermal bands to improve atmospheric correction and surface temperature accuracy, particularly over heterogeneous landscapes (Hoa *et al.* 2025). The methodological framework was harmonized across both sensors to ensure consistency in spatiotemporal comparisons and enhance the reliability of trend analysis.

LST Retrieval from Landsat 5 TM (1989)

To derive LST from Landsat 5 Thematic Mapper (TM) imagery, the widely adopted single-channel algorithm was employed, using Band 6, which captures the thermal infrared (TIR) radiation in the wavelength range of 10.4–12.5 µm. Although the native spatial resolution of Band 6 is 120 meters, it was resampled to 30 meters to ensure consistency with other spectral bands (Chander *et al.* 2009).

Step 1. Spectral radiance calculation

The top-of-atmosphere (TOA) spectral radiance (Lλ) was computed from the digital number (DN) values using the radiometric rescaling formula:

Equation 1 $$L_\lambda = \left(\frac{L_{Max}-L_{Min}}{QCal_{Max}-QCal_{Min}}\right) \times (DN - QCal_{Min}) + L_{Min}$$

where, L_{Min} and L_{Max} are minimum and maximum radiance values (sensor-specific, obtained from metadata), and typical values are: L_{Max} = 15.600, L_{MIN} = 1.238, $QCAL_{Min}$ = 1, $QCAL_{Max}$ = 255

Step 2. Brightness temperature (Kelvin)

The at-sensor brightness temperature (T_B) in Kelvin was calculated using the inverse Planck function:

Equation 2 $$T_B = \frac{K_2}{\ln\left(\frac{K_1}{L_\lambda}+1\right)}$$

where, K_1 = 607.76 W m^{-2} sr^{-1} μm^{-1}, K_2 = 1260.56 K, L_λ = Spectral radiance at the sensor's aperture Wm^{-2} sr^{-1} μm^{-1}, In = Natural logarithm

Step 3. Surface emissivity (ε) estimation

Surface emissivity (ε) was estimated using NDVI-based classification, as proposed by Sobrino *et al.* (2004) and developed by Li *et al.* (2021):

- $NDVI < 0 \rightarrow$ water or non_vegetated $\rightarrow \varepsilon \approx 0.99$
- $NDVI < 0.2 \rightarrow$ Bare soil $\rightarrow \varepsilon \approx 0.97$
- $NDVI > 0.5 \rightarrow$ Vegetation $\rightarrow \varepsilon \approx 0.99$
- $0.2 \leq NDVI \leq 0.5 \rightarrow$ Mixed Surfaces $\rightarrow \varepsilon_{mix}$

For mixed pixels ($0.2 \leq NDVI \leq 0.5$), emissivity (ε_{mix}) was estimated using NDVI-based threshold method in the Equation 3.

Equation 3 $$\varepsilon_{mix} = 0.004 \times NDVI + 0.986$$

Step 4. LST (°C)

The final LST in degrees Celsius was derived using:

Equation 4 $$LST = \frac{T_B}{1+\left(\frac{\lambda . T_B}{\rho}\right)\ln(\varepsilon)} - 273.15$$

where, λ = 11.5 μm (effective wavelength for TM Band 6) and $\rho = \frac{hc}{k} = 1.438 \times 10^{-2}\ m\ K^{-1}$ with h as Planck's constant, c = the speed of light and k the Boltzmann constant.

LST Retrieval from Landsat 8 OLI/TIRS (2023)

LST from the 2023 Landsat 8 OLI/TIRS image was calculated using the Split-Window Algorithm (Sobrino *et al.* 2016; Badapalli *et al.* 2025), which incorporates data from both thermal bands:

Equation 5 $$\mathrm{LST} = T_{B10} + 1.378(T_{B10} - T_{B11}) + 0.183(T_{B10} - T_{B11})^2 - 0.268$$

where T_{B10} and T_{B11}: brightness temperatures from Bands 10 and 11 (in Kelvin), respectively.

Prior to applying this equation, radiance values were calculated using sensor-specific gain and bias coefficients from the metadata, and brightness temperatures were obtained using Planck's law in a manner analogous to the method used for Landsat 5 TM described above. This ensured consistency in thermal data preprocessing across both time points. The split-window approach compensates for atmospheric and emissivity effects more effectively than single-band methods, offering enhanced accuracy in complex heterogeneous urban and vegetated environments.

NDVI Calculation

NDVI was computed to support surface emissivity estimation and analyze vegetation conditions using:

Equation 6 $$NDVI = \frac{NIR-RED}{NIR+RED}$$

where the Near-Infrared (NIR) and Red (RED) bands are sensor-specific. For Landsat 5 TM, Band 4 corresponds to NIR and Band 3 to RED; for Landsat 8 OLI, Band 5 represents NIR and Band 4 represents RED. NDVI values typically range between −1 and +1, with higher values indicating dense, healthy vegetation and lower values representing bare soil, built-up areas, or water bodies. This index facilitates consistent vegetation monitoring and temporal comparisons across multi-decadal satellite datasets (Gascon *et al.* 2016).

Global Moran's

To evaluate spatial autocorrelation in the distribution of LST, the Global Moran's I statistic was employed. This index is widely used due to its ability to quantify the degree of spatial clustering or dispersion of geographic phenomena (Clark & Hosking 1986; Lee & Wong 2001). A positive Moran's I value indicates spatial clustering, whereas a negative value suggests dispersion (Khosravi *et al.* 2017; Zhou *et al.* 2022). Statistical significance is assessed using the associated Z-score and *p*-value (Pandey & Kumari 2023). In this study, Moran's I was calculated using ArcGIS 10.5 to analyze spatial patterns in LST. The formulation of Moran's I is as follow:

Equation 7 $$I = \frac{n}{s_0} \times \frac{n \sum_{i=1}^{n} \sum_{j=1}^{n} w_{ij} z_i z_j}{\sum_{i=1}^{n} z_i^2}$$

where, n is the total number of spatial units, Z_i is the deviation of observation i from the mean, W_{ij} is the spatial weight between observations i and j, S_0 is the sum of all spatial weights, calculated as:

Equation 8 $$s_0 = \sum_{i=1}^{n} \sum_{j=1}^{n} wij$$

The standardized Z-score used to assess the significance of Moran's I is given by:

Equation 9 $$z_i = \frac{i - E(I)}{\sqrt{V(I)}}$$

This approach allows for robust assessment of spatial dependence in the LST data. A positive Moran's I value indicates clustering (hot/cold spots), while a negative value suggests dispersion. This spatial analysis aids in identifying thermal anomalies and land-use-driven surface dynamics (Mouton *et al.* 2022).

RESULTS

NDVI analysis

According to Fig. 2, the NDVI results for 2023 range from -0.27 to +0.65. The red areas indicate the lowest NDVI values, corresponding to regions with sparse or no vegetation cover, such as urban areas and water bodies, which often show negative NDVI values. In contrast, dark green areas represent dense vegetation, typically found in forests or pastures. For the year 1989, NDVI values ranged from -0.42 to +0.07, indicating a relatively higher vegetation cover compared to 2023. The higher negative values in 1989 are primarily associated with the broader extent of water bodies during that period.

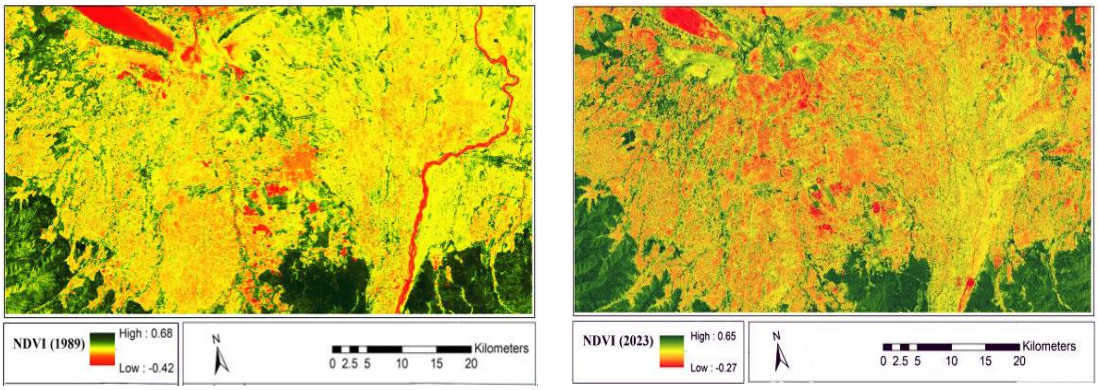

Fig. 2. NDVI map for 1989 and 2023.

NDVI trend

In 1989, the minimum NDVI value was -0.42, which increased to -0.27 in 2023. The mean NDVI value increased from 0.15 in 1989 to 0.27 in 2023. However, the maximum NDVI slightly decreased from 0.68 in 1989 to 0.65 in 2023.

LST analysis

Fig. 3 and Table 2 show the spatial distribution and descriptive statistics of LST for 1989 and 2023. The mean LST increased from 18.48 °C in 1989 to 23.13 °C in 2023.

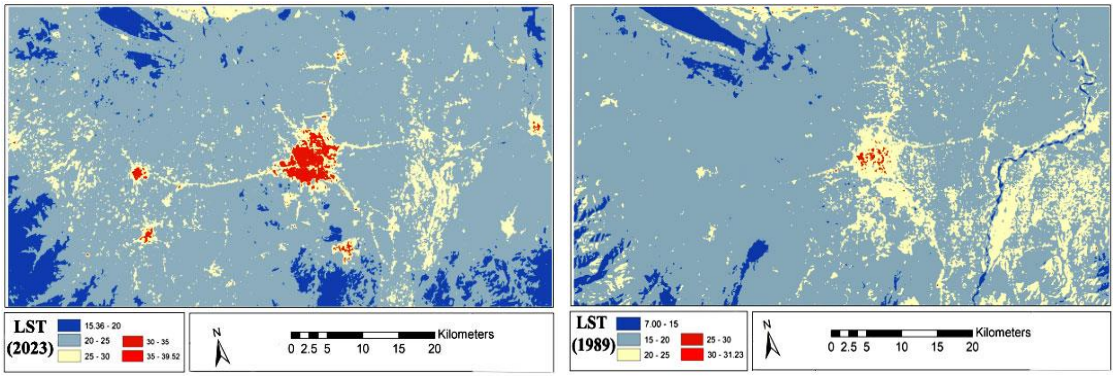

Fig. 3. LST map for 1989 2023.

LST trend

As shown in Fig. 5, changes in LST between 1989 and 2023 reveal a shift from lower temperature classes (< 20 °C) toward higher classes (20–25 °C and 25–30 °C). The most significant change occurred in areas that shifted from < 20 °C in 1989 to 20–25 °C in 2023, covering approximately 22,085 hectares. Another major change involved areas moving from < 20 °C to 25–30 °C, with a total area of 14,797 hectares. These patterns clearly indicate an upward trend in surface temperatures during the study period.

Table 2. Descriptive statistics of LST in 1989 and 2023.

Year	Mean (°C)	Maximum (°C)	Minimum (°C)	Std. Deviation (°C)
1989	18.48	31.24	7.00	1.70
2023	23.13	39.52	15.36	2.10

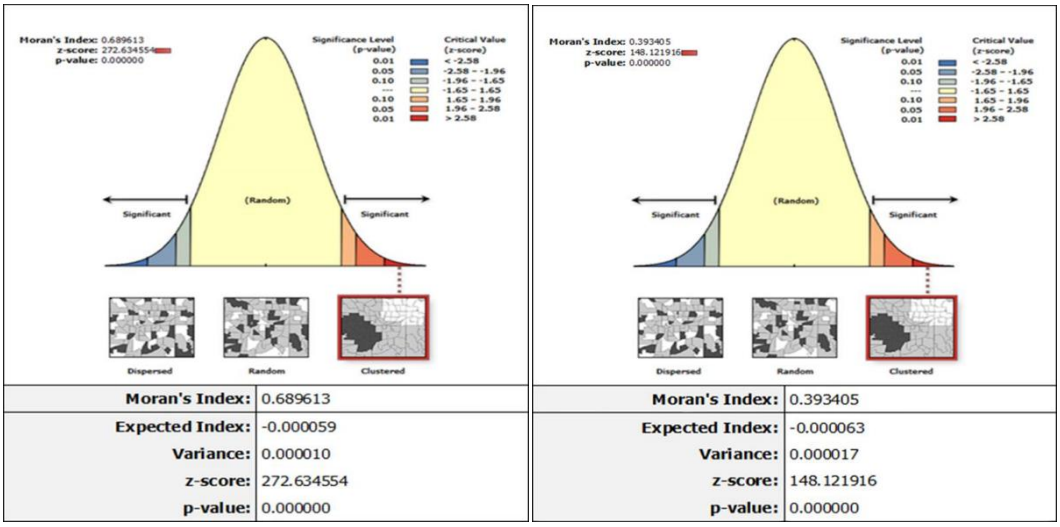

Fig. 4. Moran's I for 1989 and Moran's I for 2023.

Table 3. Pearson correlation results between LST and NDVI for 1989 and 2023.

		NDVI (2023)	LST (1989)
NDVI (1989)	Pearson Correlation	-	-0.718**
	Sig. (2-tailed)	-	0.002
LST (2023)	Pearson Correlation	-0.743**	-
	Sig. (2-tailed)	0.001	-

Note: (**) indicate statistically significance at the 0.01 level (2-tailed).

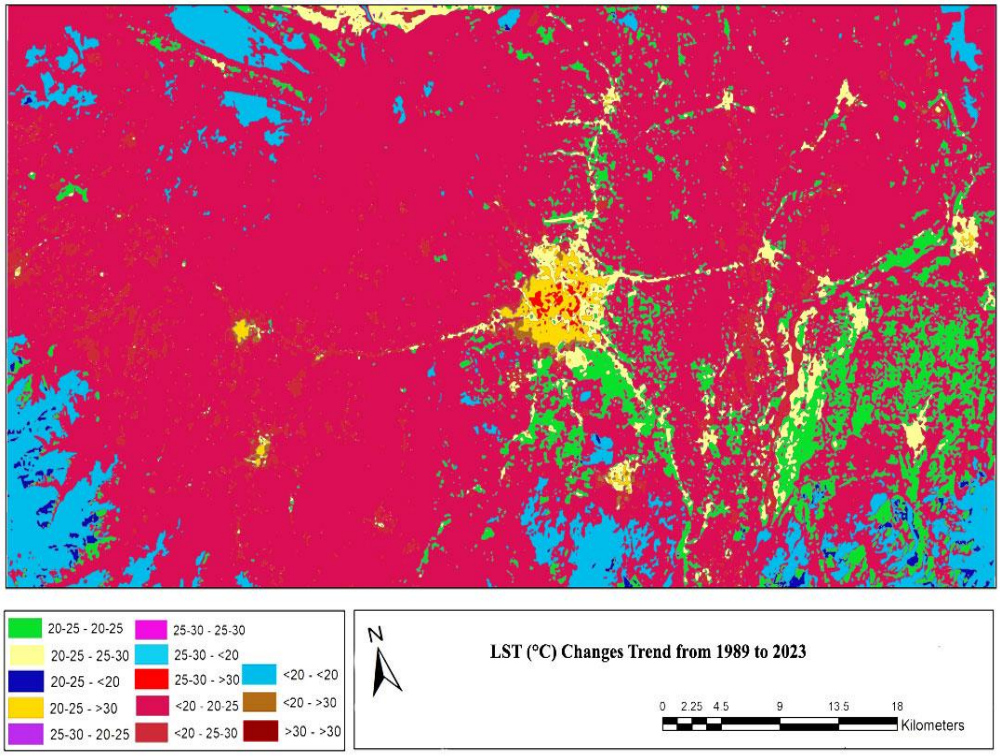

Fig. 5. Map of land surface temperature (LST) changes between 1989 and 2023.

DISCUSSION

The observed 4.65 °C increase in LST from 1989 to 2023 across Central Guilan Province provides clear evidence of a significant regional warming trend, consistent with global climate change projections (Chen *et al.* 2023; IPCC 2023). This rise reflects both atmospheric warming and localized land use changes, particularly deforestation, urbanization, and agricultural intensification, trends also reported in other humid temperate provinces of Northern Iran (Komeh *et al.* 2025; Mohammadpour Zeidi & Gerami 2025). Although the mean NDVI increased from 0.15 in 1989 to 0.27 in 2023, the maximum NDVI decreased slightly from 0.68 to 0.65. This apparent inconsistency reflects different vegetation dynamics within the study area. The rise in mean NDVI is largely associated with the expansion and intensification of agricultural and semi-vegetated lands, where moderate vegetation cover was improved due to cultivation and irrigation practices. In contrast, the decline in maximum NDVI indicates a loss of the densest and healthiest vegetation patches, particularly in natural forested areas. Thus, while more areas exhibit moderate vegetation cover, the overall quality and extent of high-density natural vegetation have declined, consistent with our conclusion of vegetation degradation in Central Guilan. A strong and statistically significant negative correlation between NDVI and LST was identified for both study years: 1989 ($r = -0.718$, $p = 0.002$) and 2023 ($r = -0.743$, $p = 0.001$). This inverse relationship reinforces the fundamental ecological principle that vegetation plays a crucial role in thermal regulation through evapotranspiration, shading, and modification of surface albedo (Sun *et al.* 2020; Palafox-Juárez *et al.* 2021). Vegetated surfaces act as natural air conditioners by dissipating solar energy, a function that is significantly compromised when green areas are replaced with impervious surfaces. The consistency of this relationship over the 34-year period suggests that the degradation of vegetative cover is a key driver of increased surface temperatures in the region. These findings echo national and international calls for preserving and expanding green infrastructure as a primary adaptation strategy in the face of accelerating climate change (Carvalho 2025). The increase in Moran's I reflects a growing spatial clustering of high LST values, signifying the intensification of UHIs and a loss of thermal heterogeneity in the landscape. This increase in spatial dependence indicates that warming is becoming more spatially consolidated, likely due to the proliferation of impervious surfaces, loss of urban vegetation, and concentration of anthropogenic heat sources (Zhou & Ren 2011). Such clustering is a critical indicator of urban ecological degradation and is commonly observed in rapidly developing urban landscapes globally (Wu *et al.* 2021). Land use and land cover changes over the past three decades have profoundly transformed the ecological structure of Central Guilan. Forests and wetlands have been systematically cleared or degraded to accommodate expanding agriculture, residential

developments, and infrastructural projects. Additionally, the depletion of surface water resources—driven by increased irrigation demands, reduced precipitation, and urban consumption—has further contributed to thermal amplification and ecological stress (Weng *et al.* 2021). These transformations reduce the landscape's capacity to buffer against heat extremes and increase vulnerability to environmental hazards such as drought, flooding, and habitat fragmentation. The integrated analysis of NDVI and LST serves as a powerful methodological approach for understanding the ecological impacts of land cover change and provides actionable insights for sustainable land management. It aligns with broader theoretical frameworks in landscape ecology that emphasize the critical role of vegetation in regulating microclimatic conditions and maintaining ecosystem resilience (Wu 2021). Furthermore, this research directly supports progress toward Sustainable Development Goals (SDGs), particularly SDG 11 (Sustainable Cities and Communities), SDG 13 (Climate Action), and SDG 15 (Life on Land), by demonstrating the vital connections between ecological integrity, climate adaptation, and sustainable urban development (United Nations 2020). Nevertheless, several limitations should be acknowledged. The thermal band resolution of Landsat, particularly the older TM sensor, imposes spatial constraints on LST accuracy. Additionally, this study relies on single-date imagery for May 1989 and May 2023, which does not capture seasonal variability or extreme temperature events. Another limitation is the lack of ground-based validation data, which restricts the ability to directly assess the accuracy of retrieved LST values. Future studies should utilize higher temporal and spatial resolution data, such as Sentinel-3 SLSTR, MODIS, or ECOSTRESS, and incorporate multi-seasonal datasets to provide a more dynamic and robust understanding of LST and vegetation trends (Smith *et al.* 2023).

CONCLUSION

In conclusion, the documented rise in LST and decline in NDVI across Central Guilan Province over the past 34 years illustrate the profound ecological impacts of land use change and urban expansion under a warming climate. The intensifying spatial autocorrelation of LST and the robust negative NDVI–LST correlation highlight the vital regulatory function of vegetation in maintaining thermal and ecological balance. These insights underscore the urgency of adopting integrated land management strategies that prioritize green infrastructure, ecological conservation, and climate-adaptive urban planning. Through a combination of scientific monitoring, policy reform, and community engagement, Central Guilan can shift toward a more sustainable, resilient, and liveable future in the face of accelerating climate change.

RECOMMENDATIONS

Based on the findings of this study, the following measures are proposed to mitigate urban warming and strengthen environmental resilience in Central Guilan:

Prioritizing urban green infrastructure (top priority): Expansion of urban forests, parks, green roofs, and vegetated corridors should be the cornerstone of climate adaptation. Such interventions are cost-effective, scalable, and directly mitigate the UHI effect while improving public health and liveability.

Protecting and restoring natural ecosystems (secondary priority): Safeguarding remaining forests and wetlands, alongside active reforestation, afforestation, and wetland restoration, is essential to stabilize microclimates, support biodiversity, and enhance carbon sequestration.

Integrating climate into land use planning: Zoning and development policies should limit encroachment into ecologically sensitive areas and embed climate-responsive urban design principles such as maximizing vegetation cover and reducing impervious surfaces.

Strengthening monitoring and community engagement: Continued monitoring with advanced LST technologies and ground data, coupled with public education and community-based initiatives (e.g., tree planting, water conservation), will build long-term capacity for adaptation.

ACKNOWLEDGMENTS

The authors acknowledge Dr. Tavakoli for his valuable support and helpful recommendations. The authors also thank Mr. Zadnemat for his assistance in preparing the preliminary draft of the manuscript.

REFERENCES

Abdollahi, S 2019, Analysis and prediction of land use changes in coastal areas of Gilan Province, Iran. *Environmental Sciences*, 17(4): 1-14, https://envs.sbu.ac.ir/article_98069.html.

Aghsaei, H, Dinan, NM, Moridi, A, Asadolahi, Z, Delavar, M, Fohrer, N & Wagner, PD 2020, Effects of dynamic land use/land cover change on water resources and sediment yield in the Anzali wetland catchment, Gilan, Iran. *Science of the Total Environment*, 712: 136449, https://doi.org/10.1016/j.scitotenv.2019.136449.

Alademomi, AS, Okolie, CJ, Daramola, OE, Akinnusi, SA, Adediran, E, Olanrewaju, HO, Alabi, AO, Salami, TJ & Odumosu, J 2022, The interrelationship between LST, NDVI, NDBI, and land cover change in a section of Lagos metropolis. *Nigeria. Applied Geomatics*, 14(2): 299-314.

Avdan, U & Jovanovska, G 2016, Algorithm for automated mapping of land surface temperature using LANDSAT 8 satellite data. *Journal of Sensors*, 2016(1): 1480307.

Azadeh, SR & Etemadi kia, H 2024, Modelling the Spatial Expansion of Urban Heat Islands in Rasht Metropolitan, *Geography and Territorial Spatial Arrangement*, 14(50): 29-54.

Badapalli, PK, Nakkala, AB, Gugulothu, S & Kottala, RB 2025, Dynamic land degradation assessment: Integrating machine learning with Landsat 8 OLI/TIRS for enhanced spectral, terrain, and land cover indices. *Earth Systems and Environment*, 9(1): 315-335.

Carvalho, R 2025, Green infrastructure planning. In: Handbook of Nature-Based Drought Solutions, Elsevier pp. 359-376.

Chander G, Markham BL, & Helder DL 2009, Summary of current radiometric calibration coefficients for Landsat MSS, TM, ETM+, and EO-1 ALI sensors. *Remote Sensing of Environment*. 113(5): 893-903.

Chen, Z, Li, X, Liu, X & Zhu, Z 2023, Assessing urban heat island dynamics and land surface temperature changes in rapidly urbanizing regions using multi-temporal remote sensing data. *Remote Sensing of Environment*, 286: 113388.

Clark, PJ & Hosking, JR 1986, Statistical methods for geographers. Wiley, New York.

Cracknell, AP 2007, Introduction to remote sensing. CRC Press.

Delgado-Capel, MJ, Egea-Cariñanos, P, & Cariñanos, P 2024, Assessing the relationship between land surface temperature and composition elements of urban green spaces during heat waves episodes in Mediterranean cities. *Forests*, 15(3): 463, https://doi.org/10.3390/f15030463

Eastman, JR 2009, IDRISI Taiga guide to GIS and image processing. Clark Labs, Clark University, Worcester, MA.

Elachi, C & Van Zyl, JJ 2021, Introduction to the physics and techniques of remote sensing. John Wiley & Sons.

Ellis, EC 2015, Ecology in an anthropogenic biosphere. *Ecological Monographs*, 85(3): 287-331.

Fallah Ghalhari, G & Dadashi Roudbari, A 2018, An investigation on thermal patterns in Iran based on spatial autocorrelation. *Theoretical and Applied Climatology*, 131(3): 865-876.

FAO 2021, The State of the World's Land and Water Resources for Food and Agriculture – Systems at breaking point. Food and Agriculture Organization, Rome.

Forman, RTT & Godron, M 1986, Landscape ecology. John Wiley & Sons, New York.

Francis, RA, Millington, JD, Perry, GL, & Mino,r ES, 2022, The Routledge handbook of landscape ecology. London: Routledge.

Gascon M, Cirach M, Martínez D, Dadvand P, Valentín A, Plasència A, Nieuwenhuijsen M 2016, Normalized difference vegetation index (NDVI) as a marker of surrounding greenness in epidemiological studies: The case of Barcelona city. *Urban Forestry & Urban Greening*, 19: 88-94.

Guha, S, & Dube, S 2021, A long-term seasonal analysis on the relationship between land surface temperature and normalized difference vegetation index in Raipur City, India. *Science of the Total Environment*, 755: 142522.

Haghighi Khomami, M, Bonyad, AE & Panahandeh, M 2023, Anzali Wetland Surface Area Evaluation Based on Landsat Time Series Data and NDWI *Indices. Iranian Journal of Soil and Water Research*, 54(1): 173-192, https://doi.org/10.22059/ijswr.2023.352988.669421.

Hoa, PV, Binh, NA, Thao, GTP, An, NN, Trinh, PT, Tuan, NQ & Hanh, NC 2025, Long-term trend and seasonal cycles of gap-free downscaled diurnal/nocturnal LST and the interaction to functional plant trait under tropical monsoon climate. *Earth and Space Science*, 12(2): e2024EA003888.

IPCC 2023, Climate Change 2023: Synthesis Report, Intergovernmental Panel on Climate Change, viewed 10 April 2025, https://www.ipcc.ch/report/ar6/syr.

Karimi Firozjaei, M, Mahmoodi, H & Jokar Arsanjani, J 2025, Daytime surface urban heat island variation in response to future urban expansion: An assessment of different climate regimes. *Remote Sensing*, 17(10): 1730.

Khosravi, R, Safari, H & Alavi, S 2017, Spatial analysis of land surface temperature using Moran's I and Geographically Weighted Regression, *Geographical Journal of Environmental Planning*, 28(4): 47–64.

Komeh, Z, Hamzeh, S, Memarian, H, Attarchi, S, & Alavipanah, SK 2025, A remote sensing approach to spatiotemporal analysis of land surface temperature in response to land use/land cover change via Cloud Base and Machine Learning methods, Case study: Sari Metropolis, Iran. *International Journal of Environmental Research*, 19(3): 98.

Lee, J & Wong, DW 2001, Statistical analysis with ArcView GIS, John Wiley & Sons, New York.

Li, X, Zhou, Y & Ouyang, W 2021, Quantifying spatial patterns of urban heat islands using spatial autocorrelation metrics: A global perspective. *Science of the Total Environment*, 782: 146859.

Lillesand, T, Kiefer, RW & Chipman, J 2015, Remote sensing and image interpretation. John Wiley & Sons.

MohammadpourZeidi, A, & Gerami, MS 2025, Analysis of urban heat islands and the effects of land use changes and its synoptic patterns (Case study: Ramsar City). *Advances in Meteorology*, 2025(1): 8876372.

Mouton, TL, Leprieur, F, Floury, M, Stephenson, F, Verburg, P & Tonkin, JD 2022, Climate and land-use driven reorganisation of structure and function in river macroinvertebrate communities. *Ecography*, 2022(3): e06148.

Naveh, Z & Lieberman, AS 1994, Landscape ecology: Theory and application. 2nd edition, Springer, New York.

Palafox-Juárez EB, López-Martínez JO, Hernández-Stefanoni JL, Hernández-Nuñez H 2021, Impact of urban land-cover changes on the spatial-temporal land surface temperature in a tropical City of Mexico. *ISPRS International Journal of Geo-Information*, 10(2):76.

Pandey S, Kumari N 2023, Prediction and monitoring of LULC shift using cellular automata-artificial neural network in Jumar watershed of Ranchi District, Jharkhand. *Environmental Monitoring and Assessment*, 195(1): 130.

Rahimi, E, Dong, P & Jung, C 2025, Global NDVI-LST correlation: Temporal and spatial patterns from 2000 to 2024. *Environments*, 12(2): 67.

Rizwan, AM & Dennis, LY 2008, A review on the generation, determination and mitigation of Urban Heat Island. *Journal of environmental Sciences*, 20(1): 120-128.

Roy, DP, Wulder, MA, Loveland, TR, Ce, W, Allen, RG, Anderson, MC, Helder, D, Irons, JR, Johnson, DM, Kennedy, R & Scambos, TA 2014, Landsat-8: Science and product vision for terrestrial global change research. *Remote Sensing of Environment*, 145: 154-172.

Santamouris, M 2020, Recent progress on urban overheating and heat island research. Integrated assessment of the energy, environmental, vulnerability and health impact. Synergies with the global climate change. *Energy and Buildings*, 207, p. 109482.

Shakiba, F, Rousta, I, Mazidi, A & Olafsson, H 2024, Spatial and temporal variation of day and night time land surface temperature and its drivers over Iran's watersheds using remote sensing. *Earth Science Informatics*, 17(4): 3567-3587.

Shooshtari, SJ & Gholamalifard, M 2015, Scenario-based land cover change modelling and its implications for landscape pattern analysis in the Neka Watershed, Iran. *Remote Sensing Applications: Society and Environment*, 1: 1-19.

Smith, J, Johnson, D & Martinez, L 2023, Enhanced spatial and temporal analysis of LST using Sentinel-3 data. *Remote Sensing Applications: Society and Environment*, 29: 100871.

Sobrino JA, Jiménez-Muñoz JC, & Paolini L 2004, Land surface temperature retrieval from LANDSAT TM 5. Remote Sensing of environment. *Remote Sensing of Environment*, 90(4): 434-440.

Sobrino JA, Jiménez-Muñoz JC, Sòria G, Ruescas AB, Danne O, Brockmann C, Ghent D, Remedios J, North P, Merchant C, Berger 2016, Synergistic use of MERIS and AATSR as a proxy for estimating Land Surface Temperature from Sentinel-3 data. *Remote Sensing of Environment*, 179: 149-161.

Statistical Centre of Iran 2016, Iran's population and housing census-2016. Retrieved from https://www.unescap.org/sites/default/files/Session6_Iran_Population_and_Housing_Census2016_Census_WS_24-26Jan2018.pdf.

Sun, Z, He, C & Li, J 2020, Vegetation's mitigation role in land surface temperature: A global analysis based on remote sensing and climate data. *Ecological Indicators*, 117: 106593.

UN 2015, Transforming our world: The 2030 agenda for sustainable development, United Nations, viewed 14 May 2025, https://sdgs.un.org/2030agenda.

UN 2018, World urbanization prospects: The 2018 revision, United Nations Department of Economic and Social Affairs, Population Division, New York.

United Nations 2020, The sustainable development goals report 2020. viewed 20 May 2025, https:// unstats.un.org/sdgs/report/2020/.

USGS 2021, Landsat science data users handbook, United States Geological Survey, viewed 12 March 2025, https://www.usgs.gov/landsat-missions.

Weng, Q 2009, Thermal infrared remote sensing for urban climate and environmental studies: Methods, applications, and trends. *ISPRS Journal of Photogrammetry and Remote Sensing*, 64(4): 335–344.

Weng, Q, Fu, P & Gao, F 2021, Modelling and understanding urban land surface temperature and its relationships with land cover types using remote sensing data. *ISPRS Journal of Photogrammetry and Remote Sensing*, 171: 35–50.

Wu J 2021, Landscape sustainability science (II): Core questions and key approaches. *Landscape Ecology*. 36(8): 2453-85.

Wu, S, Wang, P, Tong, X, Tian, H, Zhao, Y, & Luo, M 2021, Urbanization-driven increases in summertime compound heat extremes across China. *Science of the Total Environment*, 799: 149166.

Yavari, AR, Darayi, L, Hahsemi, SM & Zebardast, L 2012, Iran: A fusion of mountains and deserts. Yaran Press, Tehran, Iran.

Zhou Y, Ren G 2011, Change in extreme temperature event frequency over mainland China, 1961− 2008. *Climate Research*, 50(2-3): 125-139.

Zhou, D, Zhao, S & Zhang, L 2022, Exploring the temporal dynamics of land surface temperature and urban heat islands in expanding cities. *Environmental Research Letters*, 17(2): 024015.

Zhu, S, Li, Y, Wei, S, Wang, C, Zhang, X, Jin, X, Zhou, X & Shi, X 2022, The impact of urban vegetation morphology on urban building energy consumption during summer and winter seasons in Nanjing, China. *Landscape and Urban Planning*, 228: 104576.